ADVANCED MATERIALS
www.advmat.de

Changes of Structure and Bonding with Thickness in Chalcogenide Thin Films

Ider Ronneberger, Zeila Zanolli, Matthias Wuttig, and Riccardo Mazzarello**

Extreme miniaturization is known to be detrimental for certain properties, such as ferroelectricity in perovskite oxide films below a critical thickness. Remarkably, few-layer crystalline films of monochalcogenides display robust in-plane ferroelectricity with potential applications in nanoelectronics. These applications critically depend on the electronic properties and the nature of bonding in the 2D limit. A fundamental open question is thus to what extent bulk properties persist in thin films. Here, this question is addressed by a first-principles study of the structural, electronic, and ferroelectric properties of selected monochalcogenides (GeSe, GeTe, SnSe, and SnTe) as a function of film thickness up to 18 bilayers. While in selenides a few bilayers are sufficient to recover the bulk behavior, the Te-based compounds deviate strongly from the bulk, irrespective of the slab thickness. These results are explained in terms of depolarizing fields in Te-based slabs and the different nature of the chemical bond in selenides and tellurides. It is shown that GeTe and SnTe slabs inherit metavalent bonding of the bulk phase, despite structural and electronic properties being strongly modified in thin films. This understanding of the nature of bonding in few-layers structures offers a powerful tool to tune materials properties for applications in information technology.

The isolation of graphene from graphite in 2004 and the subsequent discovery of other stable 2D materials have opened up a new field of research. 2D materials offer plentiful opportunities for applications in information technology,[1,2] besides being of great interest for fundamental research. Progress in this field has been impressive in the past few years. Experimental techniques to produce these materials based on mechanical and chemical exfoliation, as well as chemical vapor deposition, are constantly being refined. On the computational side, high-throughput methods have come into play, offering the possibility of systematic screening to predict novel stable 2D materials.[3,4] Among the recently discovered families of 2D compounds, group IV chalcogenides (IV = Ge, Sn; chalcogen = S, Se, Te) are attracting significant interest due to their remarkable electronic properties, which include in-plane ferroelectric polarization tunable by strain engineering.[5–12]

A fundamental question arising in the study of 2D and few-layer materials is how bulk properties emerge upon increasing the film thickness. Interestingly, a number of different scenarios appear feasible. van der Waals bonded materials like graphite or multilayer graphene exhibit only a very small interlayer coupling and hence weak film thickness dependence of their properties. A stronger coupling can only be produced if adjacent bilayers are twisted, giving rise to exciting phenomena such as superconductivity in twisted graphene sheets.[13] A weak thickness dependence is expected whenever interlayer coupling is accomplished by weak van der Waals forces. On the other hand, covalently bonded materials like Si show pronounced relaxations or reconstructions at the surface to compensate for the lack of bonding partners.[14] The resulting atomic rearrangements are usually restricted to a few monolayers. Chalcogenides such as transition metal dichalcogenides also

Dr. I. Ronneberger, Prof. R. Mazzarello
Institute for Theoretical Solid State Physics
JARA-FIT and JARA-HPC
RWTH Aachen University
Aachen D-52074, Germany
E-mail: mazzarello@physik.rwth-aachen.de

The ORCID identification number(s) for the author(s) of this article can be found under https://doi.org/10.1002/adma.202001033.

[+]Present address: Debye Institute for Nanomaterials Science, Utrecht University, The Netherlands

DOI: 10.1002/adma.202001033

Dr. Z. Zanolli
Catalan Institute of Nanoscience and Nanotechnology (ICN2)
CSIC
BIST and European Theoretical Spectroscopy Facility (ETSF)
Barcelona 08193, Spain
Dr. Z. Zanolli[+]
Institute for Theoretical Solid State Physics
RWTH Aachen University
Aachen D-52074, Germany
Prof. M. Wuttig
I. Physikalisches Institut
JARA-FIT and JARA-HPC
RWTH Aachen University
Aachen 52074, Germany
E-mail: wuttig@physik.rwth-aachen.de
Prof. M. Wuttig
JARA-Institute Green IT (PGI 10)
Forschungszentrum Jülich GmbH
Jülich 52428, Germany

show van der Waals bonding between adjacent layers, hence a weak film thickness dependence of their properties can be expected. Van der Waals gaps have also been postulated for sesquichalcogenides such as Sb_2Te_3, Bi_2Te_3, and Bi_2Se_3, but the small interlayer spacing across adjacent chalcogenide layers is indicative of significant interlayer coupling.[15]

In the case of group IV chalcogenides, most such compounds display a spontaneous in-plane ferroelectric polarization in the quasi 2D limit, whereas the bulk phases are either paraelectric (e.g., GeSe, SnSe) or ferroelectric but with a polarization pointing in a different direction as compared to the 2D case (GeTe, SnTe). The change in the polarization as a function of the number of layers is closely linked to the evolution in the structure and the electronic properties of the film. In this respect, the study of group IV chalcogenides is particularly interesting because some of them (such as GeSe and SnSe) are held together by covalent bonds in their bulk state, whereas others, including GeTe and SnTe, show a unconventional form of bonding—called metavalent bonding (MVB).[15–18] MVB stems from a competition between electron delocalization as in metals, and electron localization characteristic for covalent and ionic bonding,[16] and is characterized by a unique combination of properties[18] and unusual bond breaking.[19] In MVB adjacent atoms are held together by roughly one electron, namely half of the electron pair usually employed in covalent bonding.[17] It is plausible that materials that utilize MVB in the bulk phase should feature a change in bonding upon reducing the sample dimensions, since this favors electron localization. Concomitant changes in atomic arrangement and physical properties are expected to accompany the anticipated change in bonding.

Evidence for peculiar changes in atomic and electronic structure in thin chalcogenides has been reported.[5,12,20–24] However, unambiguous evidence for changes in bonding has not been obtained so far. In this work, we investigate the properties of thin-film models of GeTe, SnTe, GeSe, and SnSe—which are representatives of the two families of group IV chalcogenides—as a function of slab thickness. At $T = 0$, bulk GeTe and SnTe form a Peierls-distorted rocksalt structure with space group $R3m$,[25] a characteristic feature of many metavalently bonded systems. On the contrary, GeSe and SnSe, which do not exhibit MVB, crystallize into an orthorhombic phase with space group $Pnma$.[25] Here we restrict ourselves to quasi-2D models that are obtained from the cubic (GeTe, SnTe) and orthorhombic (GeSe, SnSe) phase by cutting slabs perpendicular to the (001) direction (see **Figure 1**). Using the same notation as in ref. [12], we denote these two quasi-2D phases with α and γ, respectively.

The thickness of our models is varied by changing the number of bilayers (N_{BL}) from 1 up to 18. Here we define a bilayer to consist of two layers ("sublayers"), each containing atoms with similar z components (see Figure 1). This definition is more convenient for our discussion. Nonetheless we note that some authors[6] instead use the term monolayer to denote this building block.

Figure 1 summarizes the structural properties of slabs of different thickness after relaxation. The data points for every slab are shown as a function of the layer indices. They are colored as a function of N_{BL} from red for the thinnest slab to blue for the thickest one. For convenience, the layer indices are arranged in such a way that the slabs are centered around zero. We characterize the out-of-plane relaxation by computing the difference in the z component of anion and cation atoms in subsequent layers. Two distinct values denoted as z_{short} and z_{long} can be identified in the corresponding bulk phases. As for the in-plane structural features, we choose the bond distance between neighboring anion and cation atoms in the selected atomic layer. Similarly, a short and a long in-plane distance (d_{short} and d_{long}) is defined in the bulk phases. The bulk values are indicated as dashed lines in the relevant plots.

Figure 1 reveals striking differences between the GeSe and SnSe slabs on one hand and the GeTe and SnTe slabs on the other hand. The structural features in the interior of the GeSe and SnSe models converge rapidly to the corresponding bulk values for increasing N_{BL}. Only the outermost bilayers of the slabs (for $N_{BL} > 1$) display bond lengths that are distinct from the bulk reference values, which is indicative of a surface effect. Such a thickness dependence is frequently observed for covalently bonded materials, where significant atomic rearrangements are present only in the vicinity of the surface. In Figure 1, a splitting of both interlayer and in-plane distances into three values (short, long, and "surface" bonds) can be identified. These atomic rearrangements partly stem from the fact that orthorhombic GeSe and SnSe consist of atomic bilayers stacked along (001), which are separated by quasi van der Waals gaps. These results are consistent with the relaxed structural parameters for single bilayers discussed in refs. [22–24].

By contrast, the structural behavior of the GeTe and SnTe systems is characterized by pronounced changes as a function of thickness that extend over all the layers. The interior region of the thicker slabs differs strongly from the corresponding bulk features, even for slabs containing 18 bilayers. Such a behavior is neither known for covalently bonded materials nor for typical metals. A closer look at GeTe and SnTe reveals a further characteristic in the structural relaxation: upon growing film thickness the ratio between short and long nearest-neighbor distances reaches almost one in the out-of-plane direction in the interior of the film, thus increasingly deviating from the bulk value. On the contrary, the in-plane ratio is increased in comparison to the bulk values.

The peculiar structural properties of the thin films of GeTe and SnTe can be explained by the large depolarizing fields present in the initial distorted bulk-like slabs. In contrast to orthorhombic GeSe and SnSe, rhombohedral bulk GeTe and SnTe cannot be considered as layered materials, but rather as Peierls-distorted systems along the ⟨111⟩ direction. Such Peierls distortion is a consequence of the competition between electron delocalization and electron localization.[16] As a result, both GeTe and SnTe have a ferroelectric ground state in the bulk phase with spontaneous polarization P_s pointing along ⟨111⟩.[26,27] Thus, P_s has a finite component in the out-of-plane direction. The depolarizing field associated with this component destabilizes the initial rhombohedral distortions of the slab models, leading to strong relaxations of the out-of-plane distances. This relaxation would be suppressed if the depolarizing field would be compensated by an external field.[28,29] In fact, our freestanding slab models correspond to open-circuit electric boundary conditions.[30] If the slabs were sandwiched between two metallic electrodes, then the surface charges of

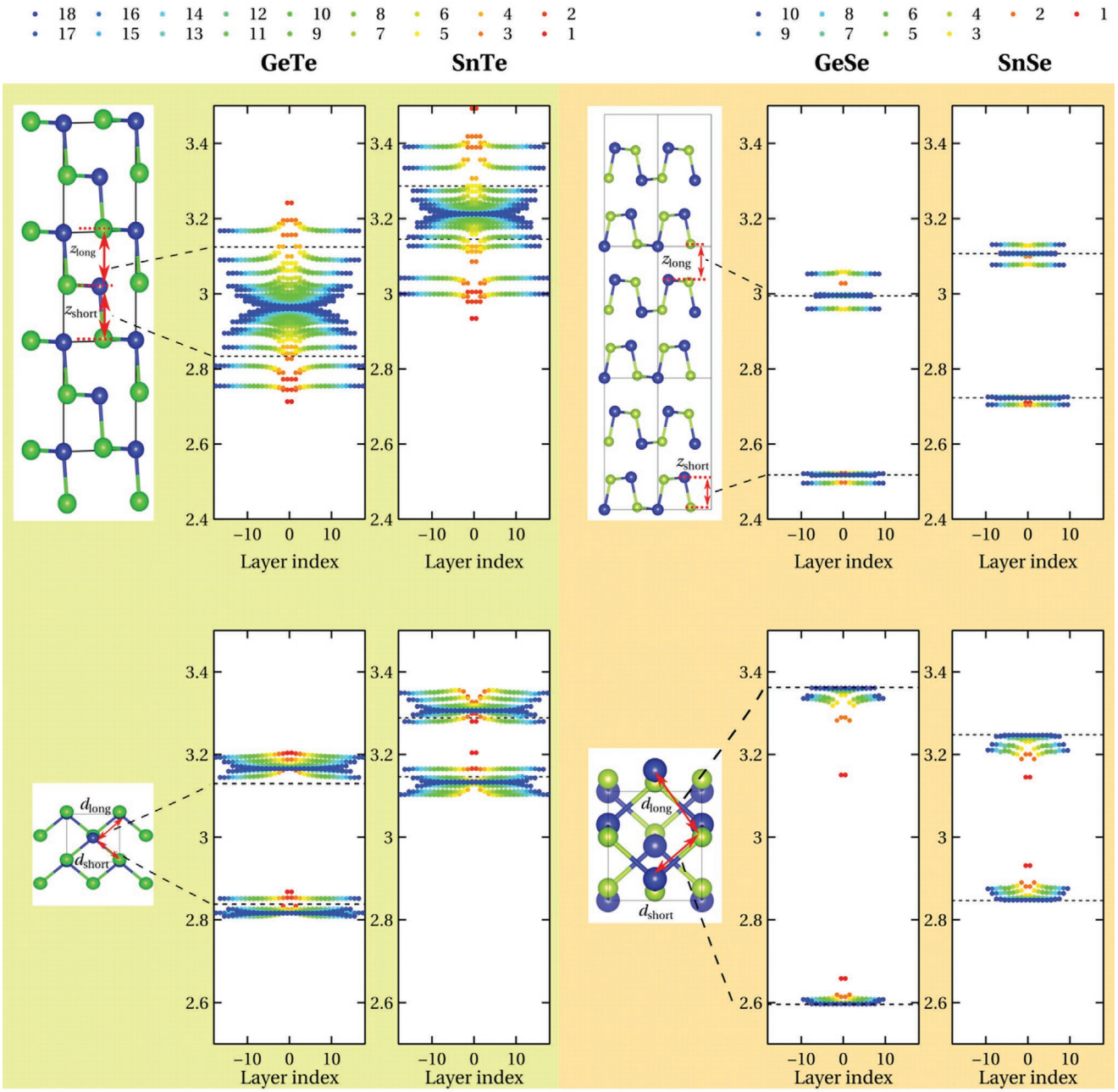

Figure 1. Out-of-plane (top) and in-plane (bottom) structural features (i.e., interlayer distance z and nearest neighbor bond distances d) as a function of the layer index. The data points are color-coded according to the thickness of the films: from red (thinnest) to blue (thickest). The two (short and long) bulk values are shown in dashed lines.

the slabs would be (partly) screened, so that the rhombohedral distortion of the bulk would be (partly) recovered. We checked this effect for one of the slab models, namely that of GeTe with $N_{BL} = 7$. The screening of the surface charges was achieved by replacing the two surface Te atoms with "pseudo" Te atoms of fractional charges counterbalancing the initial depolarizing fields.[31] As a result, bulk-like distortions in the out-of-plane direction were indeed obtained in the interior of the slab. The details of this simulation are reported in the Supporting Information.

The increase in contrast between the short and long in-plane distances originates from the suppression of the out-of-plane distortions and, thus, can be understood as an indirect effect of the depolarizing field. This very effect suggests that the in-plane component of the polarization in the thin-film models of GeTe and SnTe could be enhanced as compared to the bulk phase. From a different perspective, this effect can be rationalized by the competition between electron localization and delocalization, which characterizes MVB.[16]

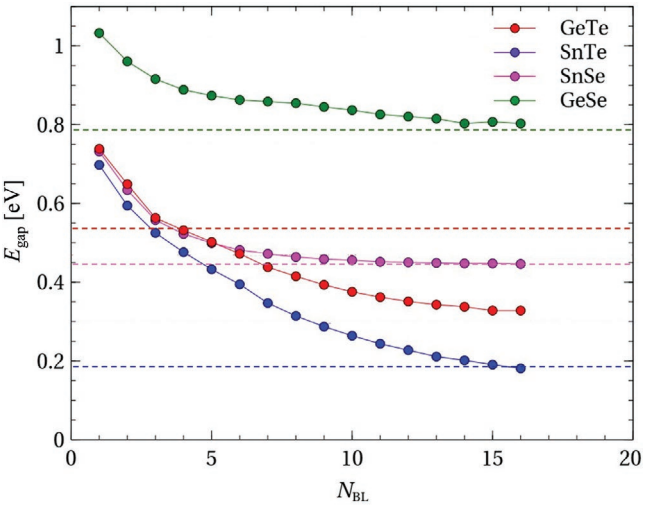

Figure 2. Bandgaps of the slabs as a function of thickness. GeTe and SnTe display more significant (absolute and relative) variations in the gap size with increasing film thickness than GeSe and SnSe.

To substantiate these claims, we turn to the discussion of the electronic and ferroelectric properties as a function of slab thickness. We have computed the spontaneous in-plane polarization P_s of all the slab models using the Berry phase approach, within the framework of the modern theory of polarization.[32,33] Further computational details are given in the Supporting Information.

The evaluation of P_s requires a finite bandgap. In **Figure 2**, the bandgaps of all the slab models are reported. Large values are found for very thin slabs, which decrease with increasing N_{BL}. The lack of smoothness of the curves stems from the fact that transitions between direct and indirect gaps occur (Figures S2 and S3, Supporting Information). For thick films, the bandgaps of the four compounds satisfy: E_{gap} (SnTe) < E_{gap} (GeTe) < E_{gap} (SnSe) < E_{gap} (GeSe). These trends are in line with the relationship between the bulk bandgaps, although it must be stressed that the bandgaps of the slab models of GeTe and SnTe do not converge to the bulk values owing to the relaxation induced by the depolarizing fields.

The absolute values of the spontaneous polarization P as function of N_{BL} are shown in **Figure 3**. In this figure, we also

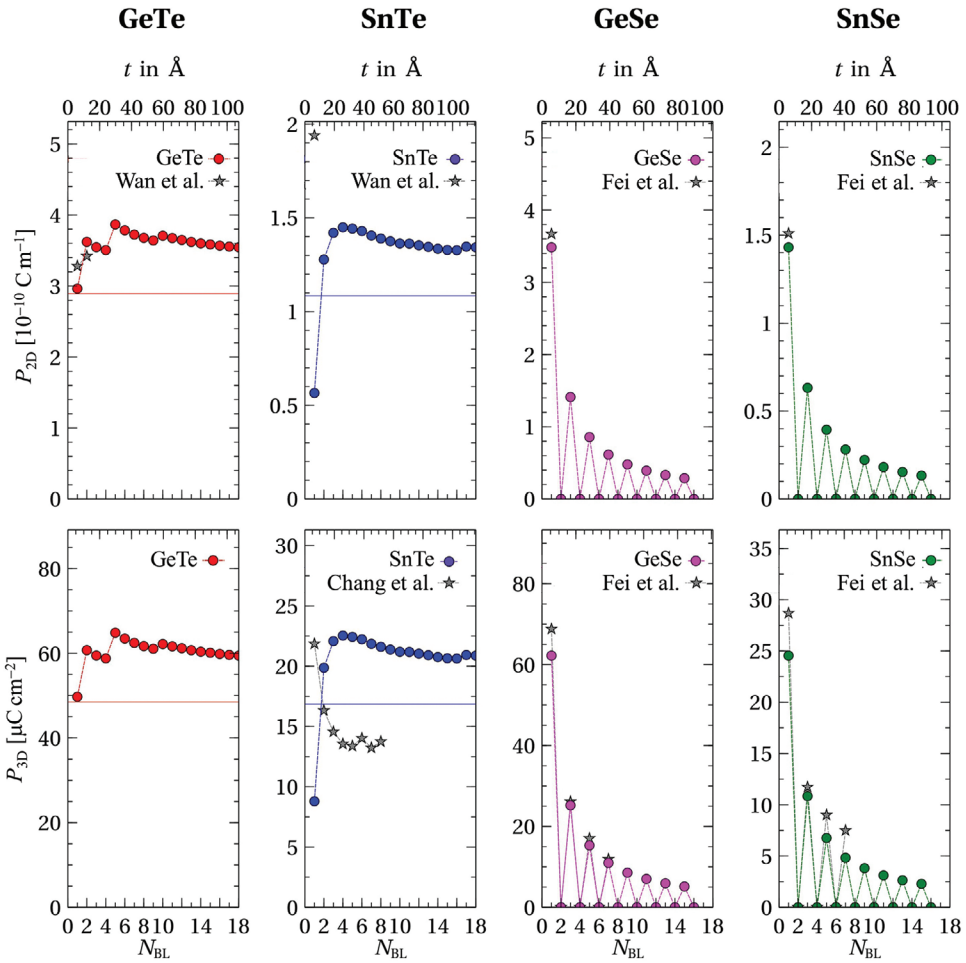

Figure 3. Spontaneous polarization P as a function of N_{BL}. The film thickness $t = t_0 \cdot N_{BL}$ (t_0 being the bulk thickness of one bilayer) is shown on the upper horizontal axis. Both 2D (top) and 3D (bottom) values of P are shown. The thin red and blue lines in the figures on the left indicate the in-plane component (along the ⟨110⟩ direction) of the bulk polarization of GeTe and SnTe, respectively. The stars refer to computational data provided in previous work, namely Chang et al.,[5] Fei et al.,[6] and Wan et al.[11]

compare our results with previous work.[5,6,11] Concerning SnTe, some discrepancies with ref. [5]—where the VASP package was used—are observed. Deviations with respect to previous VASP calculations are obtained for bulk SnTe too (Table S3, Supporting Information): these can be ascribed to the smaller cell angles obtained upon relaxation using VASP, resulting in larger Te displacements and, thus, higher polarizations. As regards GeTe, GeSe, and SnSe, there are some quantitative deviations with refs. [6,11] (due most probably to the use of different codes and pseudopotentials) but the trends are adequately reproduced. For all the models, we have verified that the polarization is computed on the same Berry-phase branch (see Supporting Information for further details). Very different behavior between GeTe/SnTe and GeSe/SnSe systems can be seen. The models of GeSe and SnSe display finite ferroelectric polarization only for odd numbers of bilayers. This is related to the mirror symmetry of two consecutive bilayers, due to which their polar displacements counterbalance each other.[6] Moreover, the absolute value of P decreases to zero as $\approx 1/N_{\mathrm{BL}}$.

In contrast to this, finite values of polarization P are obtained for all the slabs of GeTe and SnTe. As a matter of fact, this quantity becomes nearly constant for large N_{BL}. The reason for this behavior is that the structural motifs of consecutive bilayers are distorted in the same direction and the associated Berry phases do not counterbalance each other but, instead, add up. Furthermore, P shows a maximum at $N_{\mathrm{BL}} = 5$ for GeTe and $N_{\mathrm{BL}} = 4$ for SnTe. The maximal values of ≈ 65 and ≈ 23 μC cm^{-2} reached by GeTe and SnTe slabs, respectively, are not only higher than the corresponding bulk components along ⟨110⟩ (≈53.1 and ≈18.8 μC cm^{-2}), but even slightly higher than the total bulk polarizations of 60 and 21 μC cm^{-2}. This is striking observation, which is indicative for MVB as discussed in more detail below.

The Born effective charge tensor $Z^*_{s,\alpha\beta}$, defined as

$$Z^*_{s,\alpha\beta}(\mathrm{Born}) = \frac{\Omega}{e}\left.\frac{\partial P_\alpha}{\partial u_{s,\beta}}\right|_{E=0} \tag{1}$$

provides important information on the bonding properties of solids, as well as the strength of the electron–phonon coupling. In fact, large values of $Z^*_{s,\alpha\beta}$ have been shown to be fingerprints of MVB, in conjunction with other peculiar properties, such as large dielectric constants and large effective coordination numbers.[18] Instead of using the Berry-phase polarizations to estimate the $Z^*_{s,\alpha\beta}$ values, we compute the latter quantities in an independent way by employing density functional perturbation theory (DFPT).[34] In **Figure 4** the in-plane components Z^*_{xx} and Z^*_{yy} of the Born effective charge tensor for both cations (top) and anions (bottom) are shown as a function of the layer index for the ten thinnest slab models ($N_{\mathrm{BL}} = 1,\ldots,10$). As in Figure 1, the data points are color-coded according to the thickness N_{BL}.

The qualitative behavior of Z^*_{xx} and Z^*_{yy} with increasing N_{BL} is similar to the trend displayed by the in-plane distances. The Born effective charges of the GeTe and SnTe slabs in the interior region do not converge to the bulk values but, instead, show smaller absolute values. As regards GeSe and SnSe, the values of all but the outermost layers almost coincide with the bulk ones. Born effective charges are consistently larger in GeTe/SnTe as compared to GeSe/SnSe (except for the thinnest slabs of GeSe/SnSe, for which the charge values become comparable to the ones of GeTe/SnTe).

The computed values of the dynamical charges in the out-of-plane direction Z^*_{zz} are shown in the Supporting Information. These quantities are about one order of magnitude smaller than the corresponding bulk and in-plane slab values, for each material considered. This can be understood by taking into account that in the slab configurations the dynamical charges are computed under the condition of zero out-of-plane macroscopic displacement field ($D_z = 0$). The latter corresponds to the definition of Callen charge.[35] The Born effective charge is given by the product of the out-of-plane dielectric constant and the Callen charge:[35]

$$Z^*_{zz}(\mathrm{Born}) = \varepsilon^\infty_{zz} Z^*_{zz}(\mathrm{Callen}) \tag{2}$$

As discussed below, the out-of-plane dielectric constant of quasi 2D materials cannot be determined correctly from standard supercell calculations. Following ref. [36], the supercell value can be estimated using an effective-medium theory in terms of the vacuum thickness and the bulk dielectric constant as

$$\frac{1}{\varepsilon^\infty_{zz}} \approx f + \frac{1-f}{\varepsilon^\infty_{zz,\mathrm{bulk}}} \tag{3}$$

where f denotes the amount of vacuum in the supercell. The Born effective charges in the out-of-plane direction obtained in this way are of the same order of magnitude as the in-plane ones (Supporting Information). The Z^*_{zz} in the middle of the slab increase with the slab thickness, but are still smaller than the bulk values.

Going further, we use the DFPT values of the Born effective charges to validate the computed spontaneous polarization using the approximate formula

$$P \sim \frac{e}{\Omega}\sum_\beta Z^*_{s,\alpha\beta}\Delta u_{s,\beta} \tag{4}$$

where $\Delta u_{s,\beta}$ are the displacements of atom s from its centrosymmetric configuration in direction β. We find that this approach provides an accurate estimate of the polarization for the thinnest model of SnTe. However, for GeTe, the approximate formula is not accurate, due to the large magnitude of the atomic displacements.

We complete the overview of the electronic properties by computing the optical dielectric tensor ε^∞ for the same ten thinnest models. At the surface, the electronic and optical properties of materials are strongly affected by the abrupt variation of the electronic density perpendicular to the surface and the resulting fluctuations of the electric field at the atomic scale (local fields). As a consequence, periodic-boundary-condition supercell calculations fail to describe the out-of-plane optical response functions.[36] Here we only discuss the in-plane components ε^∞_{xx} and ε^∞_{yy} of the dielectric tensor. In periodic-boundary-condition calculations, their values depend on the thickness of the simulation cell, which consists of the slab and a vacuum region.[37] To compare the different 2D models we use the formula of ref. [38], in which the dielectric tensor is normalized by a geometrical thickness given by the bulk interlayer

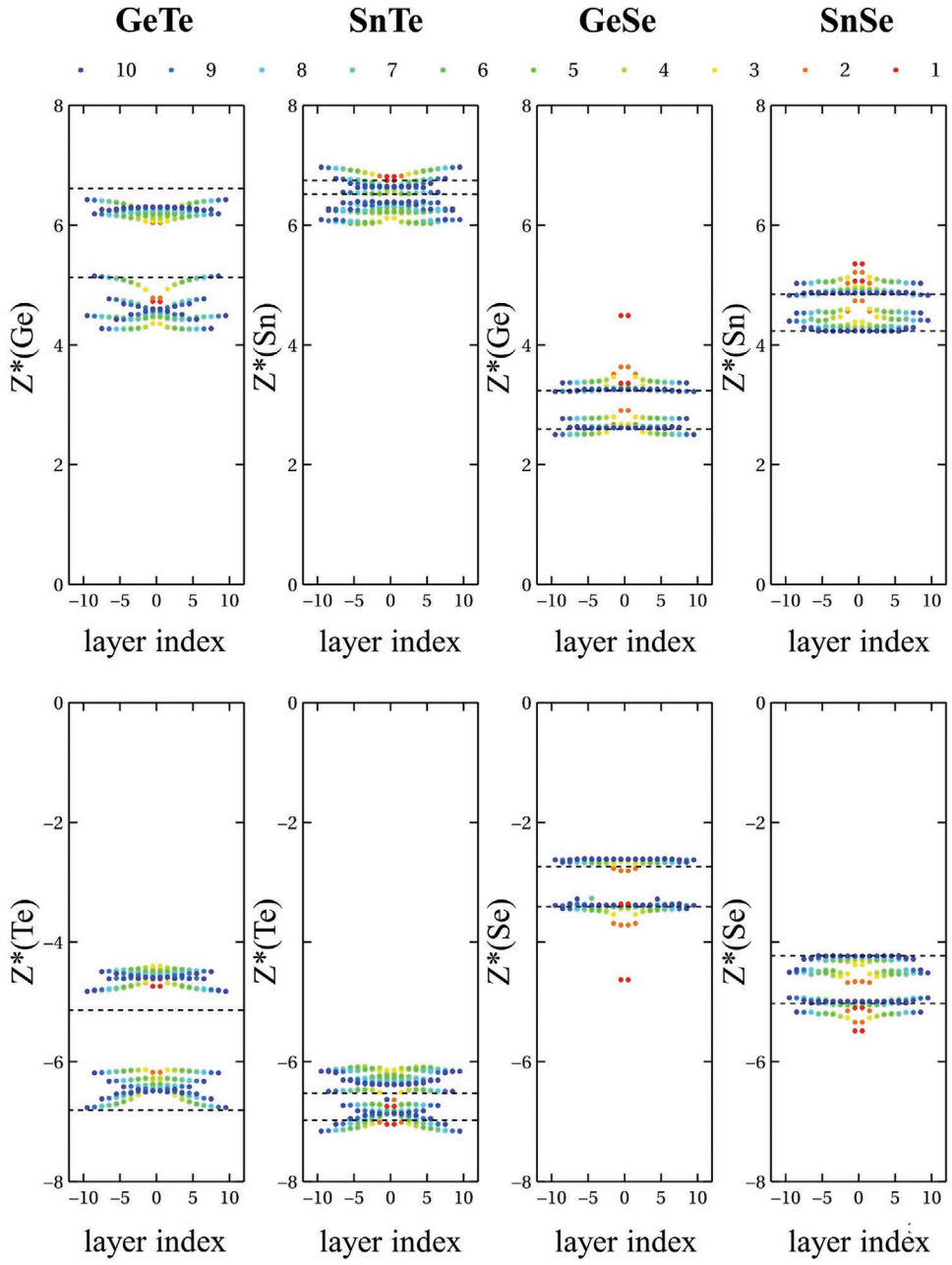

Figure 4. In-plane components of the Born effective charge tensor Z^*_{xx} and Z^*_{yy} (with $Z^*_{xx} < Z^*_{yy}$) for cations (top) and anions (bottom) as a function of the layer index. The data points are color-coded according to the thickness of the films: from red for the thinnest models to blue for the thickest models. For SnTe, distortions are rather small and the models closely approach the cubic phase: for this reason, the Z^*_{xx} and Z^*_{yy} data points almost overlap. The dashed lines correspond to the bulk values.

distance (defined as the bulk lattice constant along z divided by 2). This approach properly describes transition metal dichalcogenides, where the 2D dielectric constant weakly depends on the thickness of the quasi 2D material. In monochalcogenides, however, this dependence is more complex: Dewandre et al.[23] have shown that the effective dielectric thickness is not proportional to the geometric thickness.

The two components $\varepsilon^{\infty}_{xx}$ and $\varepsilon^{\infty}_{yy}$ are plotted as a function of N_{BL} in **Figure 5**. Again a similar trend is observed regarding the convergence toward the bulk. The values for GeTe/SnTe slabs lie below the corresponding bulk values and slowly increase with N_{BL}. The moderate difference in ε^{∞} between GeTe/SnTe slabs and the bulk models suggests that they have a similar in-plane bonding state. In contrast, thin films of GeSe and SnSe have much lower values of ε^{∞}, which is indicative of covalent bonding. Interestingly, the thinnest films of GeSe/SnSe show significantly enhanced values of ε^{∞}, although the bulk values are recovered quickly.

The unusual structural properties of the α models of GeTe and SnTe call for a detailed study of their bonding mechanism.

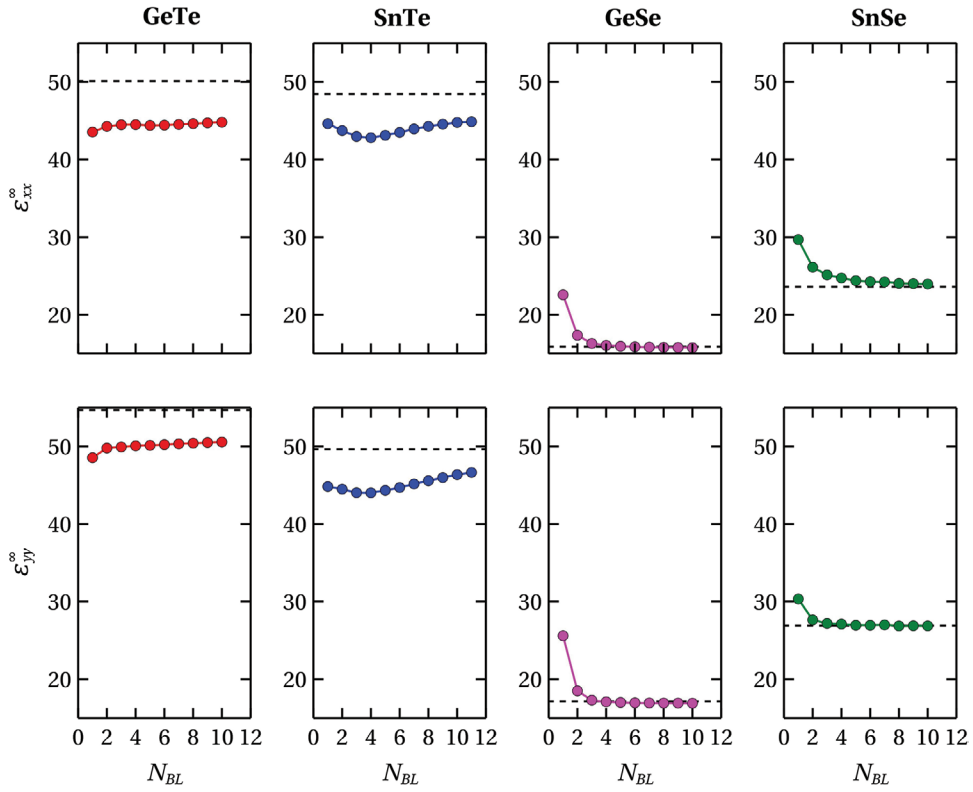

Figure 5. The in-plane components of the optical dielectric tensor ε^{∞} as a function of film thickness. Bulk values are shown as dashed lines.

In their bulk state, GeTe and SnTe show a peculiar combination of physical properties that have been attributed to MVB, namely: strong anharmonicities, moderate electronic conductivity, large effective coordination numbers breaking the 8-*N* rule, large values of Born effective charges and dielectric constants.[18] On the contrary, the properties of GeSe and SnSe are compatible with ordinary covalent bonding.[18] As displayed in Figures 4 and 5, there is a remarkable dependence of the latter properties on slab thickness for GeTe and SnTe, but not for the Se-based compounds. This raises the question if and how the nature of the bonding changes with film thickness.

It has recently been demonstrated that bonding in crystals can be defined and characterized employing two fundamental indicators: the electron transfer and the number of electrons shared between pairs of neighboring atoms.[17] An electron sharing between neighboring atoms equal to 2 corresponds to the Lewis picture of a perfect covalent bond. In contrast, MVB is characterized by electron-sharing values close to 1 and small amounts of electron transfer (significantly below 1.0). These conditions reflect a substantial amount of electron delocalization, yet do not imply metallic properties. The electron transfer is determined from ab initio quantum-mechanical calculations by integrating the net charge density of an atom over its basin and subtracting the charge of the free reference atom.[39] The electron sharing is obtained from the so called delocalization indices.[40] Here we employ these two indicators to investigate the bonding mechanisms in our quasi 2D models. For this purpose, we use the package critic2,[41] in which the delocalization indices are computed using an efficient technique based on maximally localized Wannier functions[42] (additional information is provided in the Computational Details section).

The computed electron-transfer values hardly depend on the film thickness. The charge-transfer values for $N_{BL} \geq 3$ are 0.44, 0.62, 0.82, and 0.80 for GeTe, SnTe, GeSe, and SnSe, respectively, in quantitative agreement with the electron transfer in the corresponding bulk phases (Supporting Information). We now focus the analysis on the electron sharing data (**Figure 6**): different values of this bond indicator are obtained for different atomic layers and, for each layer, for in-plane or out-of-plane bonds. In addition, Peierls-distorted systems possess short and long bonds. Here we consider only "short-bond" data because the sum of the electrons in the short and long-bonds is constant upon Peierls distortion. Similarly to the trends in the structural properties, the electron sharing in the interior of thin films of the selenides quickly converges to the bulk values upon increasing thickness. In contrast, the GeTe rhombohedral bulk value (upper dashed line in Figure 6) is not recovered in the slab models, not even in the thickest ones. More specifically, the larger in-plane distortion in the thin-film models of GeTe and SnTe leads to shorter bonds and more pronounced in-plane electron sharing compared to the bulk values, whereas the absence of out-of-plane distortion in the center of the slabs yields small corresponding electron-sharing values.

It is interesting that the two families of monochalcogenides behave so differently. It has recently been shown that GeTe and SnTe exhibit MVB, while GeSe and SnSe are characterized by covalent bonding.[17] This classification is based on the significant difference in the values of electron sharing between the

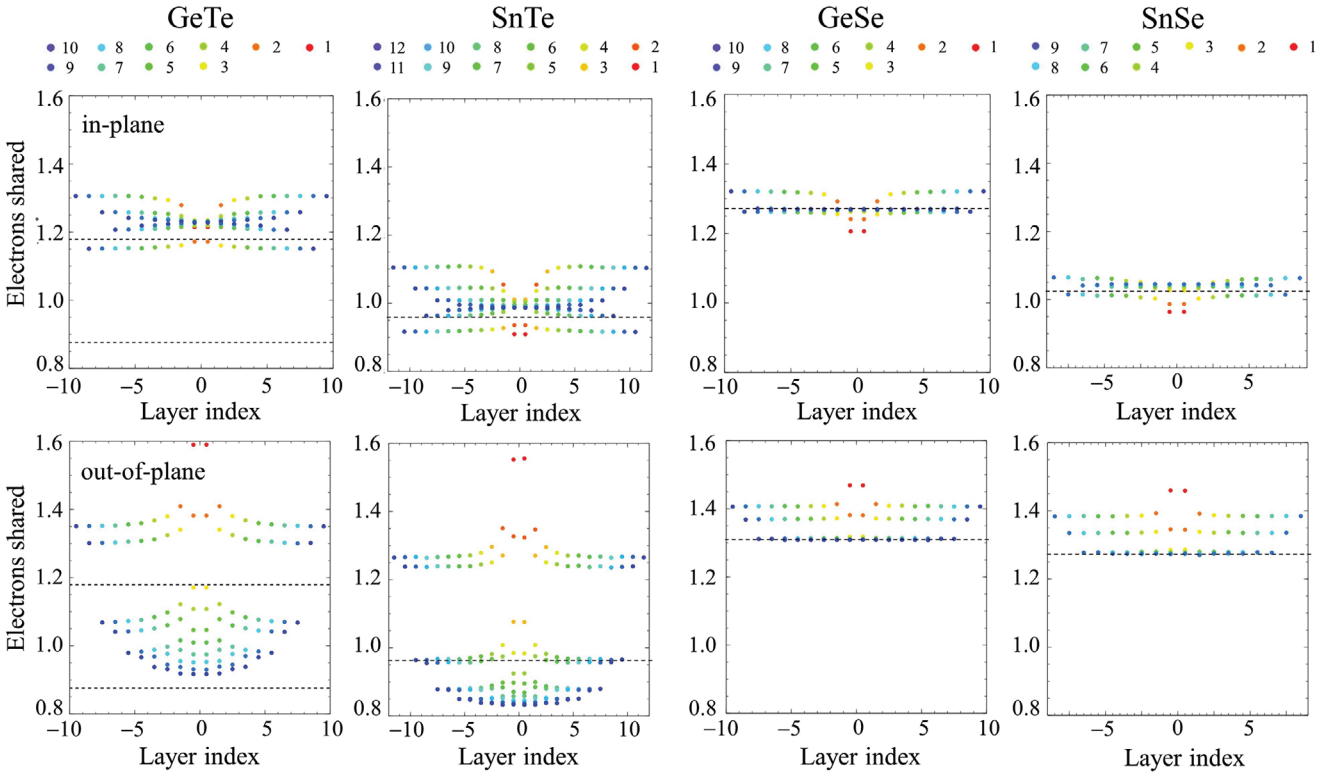

Figure 6. Amount of electrons shared between pairs of atoms in the thin-film models of GeTe, SnTe, GeSe, and SnSe. For each compound, the upper and lower plots correspond to in-plane and out-of-plane pairs of atoms, respectively. The dashed lines indicate the bulk values of this bond indicator. For GeTe, the two dashed lines correspond to the rhombohedral (higher value) and to the cubic (lower value) phase. For bulk GeSe and SnSe, the in-plane and out-of-plane electron-sharing values are different.

two families. On the contrary, the charge transfer values are relatively small in all of the four compounds. This trend can be seen even more clearly from the map of ref. [16], where the normalized electron transfer is considered, which is obtained by dividing the absolute charge transfer by the formal oxidation state. The corresponding values for the four monochalcogenides discussed here are GeTe (0.17), GeSe (0.325), SnTe (0.313), and SnSe (0.41). This moderate charge transfer is not compatible with ionic bonding.

These two different classes of monochalcogenides also show pronounced differences in the thickness dependence of their structure, their electronic properties and their bonding. The data displayed in Figure 6 underscore the different behavior of Se-based compounds, compared with Te-based systems: for GeSe and SnSe, 4 BLs can be considered as a minimal thickness for recovering the bulk in-plane and out-of-plane bond-indicator values in the central layers of the slabs. In fact, for such thicknesses, the bulk limit is obtained for all but the outermost two layers of the slabs. In contrast, in GeTe and SnTe, even the 10 BL stacks have not reached bulk values. The thinnest models (1–4 BLs) possess out-of-plane electron sharing values and structural parameters compatible with covalent bonding. However, for thicker models, about 0.9 electrons are shared between adjacent atoms along the vertical direction in the slab center. This value is close to the one of the cubic phase. Hence, there is no Peierls distortion in this direction, in agreement with the data on the film structure displayed in Figure 1. This is indicative for a more pronounced electron delocalization, in line with the more "metallic" structure. At the same time, a more significant Peierls distortion in the parallel direction (film plane) is observed. This in-plane distortion is so pronounced that the total polarization is larger for the thin film models. These findings are very plausible for a system that displays MVB and exemplify the impact of reduced dimensions on the competition between electron localization and delocalization.

Such impact is even more dramatic in ultrathin buckled films (1–4 BLs) of GeTe[20] obtained by cutting slabs perpendicular to the (111) direction of the bulk phase. These films form a layered structure consisting of alternating short and long bonds. For such systems, the reduced dimensionality suppresses electron delocalization and leads to both in-plane and out-of-plane covalent bonding.[20] Therefore, the nature of the bonding in the 2D limit also depends on the orientation of the slab. Interestingly, ultrathin slabs of SnTe (4–8 layers) grown along (001) on graphene can form a γ-phase similar to the GeSe phase,[12] which may display covalent bonding, in contrast to the α-phase. Hence, the reduced dimensionality can increase electron localization and even destabilize MVB.

In perspective, we expect that metavalently bonded materials generally exhibit unusual properties in the quasi 2D limit. Depending on the film thickness and the crystallographic direction relative to the bonding configuration, the nature of the bonding can be tuned, enhancing the versatility of these materials for applications in nanoelectronics and information

technology. For instance, few-layer Pb-based compounds (PbS, PbSe, PbTe), which are metavalently bonded in the bulk, could show analogous bonding properties as GeTe and SnTe. The behavior of thin films of Sb could also resemble the one of these tellurides, due to the similar bonding configuration in the bulk: this point could be relevant to the understanding of monatomic phase-change memories based on nanoconfined Sb.[43–45] On the contrary, covalently bonded materials such as selenides are generally less sensitive to the dimensionality reduction. Few-layer monochalcogenides are thus an excellent playground to investigate bonding in 2D materials, and the interplay between dimensionality and electronic localization.

In conclusion, we have shown that, for quasi-2D γ models of GeSe and SnSe, bulk properties—including bond lengths, dielectric constants, and bonding indicators—are recovered in the interior of slab models containing just a few bilayers. On the other hand, the structure of thin films of GeTe and SnTe shows pronounced deviations from the bulk phases, even for thicknesses exceeding 18 bilayers. We have explained this behavior in terms of strong depolarizing fields in GeTe and SnTe films and the different nature of the chemical bond in selenides and tellurides. As a result, the two groups of materials also exhibit different ferroelectric properties. Thin films of GeSe and SnSe arrange themselves in such a way that consecutive, quasi van der Waals-coupled bilayers are mirror symmetric. Hence, the polar displacements counterbalance each other.[5] In contrast, GeTe and SnTe adopt a structure where consecutive bilayers are distorted in the same direction and polarizations add up. However, the strong depolarizing fields due to the out-of-plane component of the polarization relax the slabs away from the bulk structure. As far as bonding properties are concerned, we have shown that the GeSe and SnSe γ-phase models exhibit covalent bonding similarly to the bulk phase, whereas the α-phase models of SnTe and GeTe do not approach the bulk behavior upon increasing thickness. Instead, they show full out-of-plane electron delocalization, which results in increased in-plane Peierls distortion. This peculiar behavior is a fingerprint of MVB in these materials. We thus expect similar effects when thin films of the metavalently bonded PbSe and PbTe are considered. It was recently shown that sesqui-chalcogenides such as Sb_2Te_3, Bi_2Te_3, and Bi_2Se_3 also display the characteristic features of metavalent bonding.[15] Yet, these materials are markedly more anisotropic compared with GeTe and SnTe. Therefore, it is possible that this anisotropy could lead to a different scenario in the thin-film limit: this is a very interesting point for further studies, given the significance of these sesqui-chalcogenides for thermoelectrics and as topological insulators.

Computational Details

Most of the calculations were performed using the plane wave code pw.x included in the Quantum Espresso package.[46] Additional test calculations were performed using ABINIT.[47] A vacuum region of thickness ≈15 Å was added to decouple the periodic images of the slabs. Using this vacuum region, the spurious interaction between surfaces was found to be negligible, even without applying dipole corrections. The threshold on the forces and stress components was set to 0.0005 eV Å^{-1} and 0.05 kbar, respectively. Scalar relativistic ultrasoft and norm-conserving pseudopotentials were employed and the generalized gradient approximation by Perdew, Burke, and Ernzerhof (PBE)[48] of the exchange-correlation functional was used. Semiempirical van der Waals corrections[49] were included for the GeTe, GeSe, and SnSe systems but not for SnTe, since these corrections do not properly describe the rhombohedral distortion. It is verified that the structural trends shown in Figure 1 do not depend on the details of the functional by performing geometry relaxation for selected slab models of SnTe using two widely employed van der Waals functionals (see Supporting Information). Further computational details on the Berry phase and bond-indicator calculations are provided in the Supporting Information.

Supporting Information

Supporting Information is available from the Wiley Online Library or from the author.

Acknowledgements

I.R. and Z.Z. contributed equally to this work. The authors acknowledge useful discussions with M. Stengel, M. Pohlmann, M. Kaminski and T. Sohier. M.W. and R.M. also acknowledge the computational resources granted by JARA-HPC from RWTH Aachen University under projects JARA0150, JARA0183 and JARA0198, as well as funding by the Deutsche Forschungsgemeinschaft (DFG) within the collaborative research center SFB 917 "Nanoswitches". Z.Z. acknowledges financial support by the Ramon y Cajal program RYC-2016-19344 (MINECO/AEI/FSE, UE), the CERCA programme of the Generalitat de Catalunya (Grant 2017SGR1506), the Severo Ochoa programme (MINECO, SEV-2017-0706), and by the DFG Grant No. ZA 780/3-1.

Conflict of Interest

The authors declare no conflict of interest.

Keywords

2D materials, ferroelectricity, metavalent bonding, monochalcogenides

Received: February 13, 2020
Revised: April 18, 2020
Published online: June 14, 2020

[1] K. S. Novoselov, V. I. Fal'ko, L. Colombo, P. R. Gellert, M. G. Schwab, K. Kim, *Nature* **2012**, *490*, 192.
[2] K. S. Novoselov, A. Mishchenko, A. Carvalho, A. H. Castro Neto, *Science* **2016**, *353*, 461.
[3] M. Mounet, M. Gibertini, P. Schwaller, D. Campi, A. Merkys, A. Marrazzo, T. Sohier, I. E. Castelli, A. Cepellotti, G. Pizzi, N. Marzari, *Nat. Nanotechnol.* **2018**, *13*, 246.
[4] S. Haastrup, M. Strange, M. Pandey, T. Deilmann, P. S. Schmidt, N. F. Hinsche, M. N. Gjerding, D. Torelli, P. M. Larsen, A. C. Riis-Jensen, J. Gath, K. W. Jacobsen, J. J. Mortensen, T. Olsen, K. S. Thygesen, *2D Mater.* **2018**, *5*, 042002.

[5] K. Chang, J. Liu, H. Lin, N. Wang, K. Zhao, A. Zhang, F. Jin, Y. Zhong, X. Hu, W. Duan, Q. Zhang, L. Fu, Q.-K. Xue, X. Chen, S.-H. Ji, *Science* **2016**, *353*, 274.
[6] R. Fei, W. Kang, L. Yang, *Phys. Rev. Lett.* **2016**, *117*, 097601.
[7] P. Z. Hanakata, A. Carvalho, D. K. Campbell, H. S. Park, *Phys. Rev. B* **2016**, *94*, 035304.
[8] M. Mehboudi, B. M. Fregoso, Y. Yang, W. Zhu, A. van der Zande, J. Ferrer, L. Bellaiche, P. Kumar, S. Barraza-Lopez, *Phys. Rev. Lett.* **2016**, *117*, 246802.
[9] M. Wu, X. C. Zeng, *Nano Lett.* **2016**, *16*, 3236.
[10] H. Wang, X. F. Qian, *2D Mater.* **2017**, *4*, 015042.
[11] W. Wan, C. Liu, W. Xiao, Y. Yao, *Appl. Phys. Lett.* **2017**, *111*, 132904.
[12] K. Chang, T. P. Kaloni, H. Lin, A. Bedoya-Pinto, A. K. Pandeya, I. Kostanovskiy, K. Zhao, Y. Zhong, X. Hu, Q.-K. Xue, X. Chen, S.-H. Ji, S. Barraza-Lopez, S. S. P. Parkin, *Adv. Mater.* **2018**, *31*, 1804428.
[13] Y. Cao, V. Fatemi, A. Demir, S. Fang, S. L. Tomarken, J. Y. Luo, J. D. Sanchez-Yamagishi, K. Watanabe, T. Taniguchi, E. Kaxiras, R. C. Ashoori1, P. Jarillo-Herrero, *Nature* **2018**, *556*, 80.
[14] G. Binnig, H. Rohrer, Ch. Gerber, E. Weibel, *Phys. Rev. Lett.* **1983**, *50*, 120.
[15] Y. Cheng, O. Cojocaru-Mirédin, J. Keutgen, Y. Yu, M. Küpers, M. Schumacher, P. Golub, J.-Y. Raty, R. Dronskowski, M. Wuttig, *Adv. Mater.* **2019**, *31*, 1904316.
[16] B. J. Kooi, M. Wuttig, *Adv. Mater.* **2020**, *32*, 1908302.
[17] J.-Y. Raty, M. Schumacher, P. Golub, V. L. Deringer, C. Gatti, M. Wuttig, *Adv. Mater.* **2019**, *31*, 1806280.
[18] M. Wuttig, V. L. Deringer, X. Gonze, C. Bichara, J.-Y. Raty, *Adv. Mater.* **2018**, *30*, 1803777.
[19] M. Zhu, O. Cojocaru-Mirédin, A. M. Mio, J. Keutgen, M. Küpers, Y. Yu, J. Y. Cho, R. Dronskowski, M. Wuttig, *Adv. Mater.* **2018**, *30*, 1706735.
[20] R. Wang, W. Zhang, J. Momand, I. Ronneberger, J. E. Boschker, R. Mazzarello, B. J. Kooi, H. Riechert, M. Wuttig, R. Calarco, *NPG Asia Mater.* **2017**, *9*, e396.
[21] B. J. Kooi, B. Noheda, *Science* **2016**, *353*, 221.
[22] T. P. Kaloni, K. Chang, B. J. Miller, Q. K. Xue, X. Chen, S. H. Ji, S. S. P. Parkin, S. Barraza-Lopez, *Phys. Rev. B* **2019**, *99*, 134108.
[23] A. Dewandre, M. J. Verstraete, N. Grobert, Z. Zanolli, *J. Phys. Mater.* **2019**, *2*, 044005.
[24] S. P. Poudel, J. W. Villanova, S. Barraza-Lopez, *Phys. Rev. Mater.* **2019**, *3*, 124004.
[25] P. B. Littlewood, *J. Phys. C: Solid State Phys.* **1980**, *13*, 4855.
[26] D. Di Sante, P. Barone, R. Bertacco, S. Picozzi, *Adv. Mater.* **2013**, *25*, 509.
[27] E. Plekhanov, P. Barone, D. Di Sante, S. Picozzi, *Phys. Rev. B* **2014**, *90*, 161108(R).
[28] B. Meyer, D. Vanderbilt, *Phys. Rev. B* **2001**, *63*, 205426.
[29] M. Stengel, N. A. Spaldin, D. Vanderbilt, *Nat. Phys.* **2009**, *5*, 304.
[30] J. Junquera, P. Ghosez, *Nature* **2003**, *422*, 506.
[31] M. Stengel, P. Aguado-Puente, N. A. Spaldin, J. Junquera, *Phys. Rev. B* **2011**, *83*, 235112.
[32] R. D. King-Smith, D. Vanderbilt, *Phys. Rev. B* **1993**, *47*, 1651.
[33] R. Resta, D. Vanderbilt, *Physics of Ferroelectrics*, Springer, Berlin, Germany **2007**.
[34] S. Baroni, S. de Gironcoli, A. Dal Corso, P. Giannozzi, *Rev. Mod. Phys.* **2001**, *73*, 515.
[35] Ph. Ghosez, J.-P. Michenaud, X. Gonze, *Phys. Rev. B* **1998**, *58*, 6224.
[36] N. Tancogne-Dejan, C. Giorgetti, V. Véniard, *Phys. Rev. B* **2015**, *92*, 245308.
[37] K. S. Thygesen, *2D Mater.* **2017**, *4*, 022004.
[38] L. C. Gomes, A. Carvalho, *Phys. Rev. B* **2015**, *92*, 085406.
[39] F. W. Bader, *Atoms in Molecules - A Quantum Theory*, Oxford University Press, Oxford, UK **1990**.
[40] R. F. Bader, M. E. Stephens, *J. Am. Chem. Soc.* **1975**, *97*, 7391.
[41] A. Otero-de-la-Roza, Á. M. Pendás, E. R. Johnson, *J. Chem. Theory Comput.* **2018**, *14*, 4699.
[42] N. Marzari, D. Vanderbilt, *Phys. Rev. B* **1997**, *56*, 12847.
[43] M. Salinga, B. Kersting, I. Ronneberger, V. P. Jonnalagadda, X. T. Vu, M. Le Gallo, I. Giannopoulos, O. Cojocaru-Mirédin, R. Mazzarello, A. Sebastian, *Nat. Mater.* **2018**, *17*, 681.
[44] W. Zhang, E. Ma, *Nat. Mater.* **2018**, *17*, 654.
[45] W. Zhang, R. Mazzarello, M. Wuttig, E. Ma, *Nat. Rev. Mater.* **2019**, *4*, 150.
[46] P. Giannozzi, S. Baroni, N. Bonini, M. Calandra, R. Car, C. Cavazzoni, D. Ceresoli, G. L. Chiarotti, M. Cococcioni, I. Dabo, A. D. Corso, S. D. Gironcoli, S. Fabris, G. Fratesi, R. Gebauer, U. Gerstmann, C. Gougoussis, A. Kokalj, M. Lazzeri, L. Martin-Samos, N. Marzari, F. Mauri, R. Mazzarello, S. Paolini, A. Pasquarello, L. Paulatto, C. Sbraccia, S. Scandolo, G. Sclauzero, A. P. Seitsonen, A. Smogunov, P. Umari, R. M. Wentzcovitch, *J. Phys.: Condens. Matter.* **2009**, *21*, 395502.
[47] X. Gonze, B. Amadon, P.-M. Anglade, J.-M. Beuken, F. Bottin, P. Boulanger, F. Bruneval, D. Caliste, R. Caracas, M. Côté, T. Deutsch, L. Genovese, P. Ghosez, M. Giantomassi, S. Goedecker, D. R. Hamann, P. Hermet, F. Jollet, G. Jomard, S. Leroux, M. Mancini, S. Mazevet, M. J. T. Oliveira, G. Onida, Y. Pouillon, T. Rangel, G.-M. Rignanese, D. Sangalli, R. Shaltaf, M. Torrent, M. J. Verstraete, G. Zerah, J. W. Zwanziger, *Comp. Phys. Commun.* **2009**, *180*, 2582.
[48] J. P. Perdew, K. Burke, M. Ernzerhof, *Phys. Rev. Lett.* **1996**, *77*, 3865.
[49] S. Grimme, *J. Comp. Chem.* **2006**, *27*, 1787.